minerals

MDPI

Article

Interlayer-Confined Cu(II) Complex as an Efficient and Long-Lasting Catalyst for Oxidation of H_2S on Montmorillonite

Elena Castellini [1,*], Fabrizio Bernini [1], Lorenzo Sebastianelli [1], Claro Ignacio Sainz-Díaz [2], Aida Serrano [3,4], German R. Castro [3,5], Daniele Malferrari [1], Maria Franca Brigatti [1] and Marco Borsari [1]

1 Department of Chemical and Geological Sciences, University of Modena and Reggio Emilia, Via Campi 103, I-41125 Modena, Italy; fabrizio.bernini@unimore.it (F.B.); lorenzosebastianelli1@gmail.com (L.S.); daniele.malferrari@unimore.it (D.M.); mariafranca.brigatti@unimore.it (M.F.B.); marco.borsari@unimore.it (M.B.)

2 Instituto Andaluz de Ciencias de la Tierra (CSIC-UGR), Av. de las Palmeras, 4, 18100 Armilla, Granada, Spain; ignacio.sainz@iact.ugr-csic.es

3 SpLine, Spanish CRG BM25 Beamline at The European Synchrotron (The ESRF), 71 Avenue des Martyrs, F-38000 Grenoble, France; aida.serrano@icv.csic.es (A.S.); german.castro@esrf.fr (G.R.C.)

4 Instituto de Cerámica y Vidrio (ICV), Consejo Superior de Investigaciones Científicas (CSIC), Kelsen 5, E-28049 Madrid, Spain

5 Instituto de Ciencia de Materiales de Madrid (ICMM), Consejo Superior de Investigaciones Científicas (CSIC), Sor Juana Inés de la Cruz 3, E-28049 Madrid, Spain

* Correspondence: elena.castellini@unimore.it; Tel.: +39-0592058679

Received: 24 April 2020; Accepted: 27 May 2020; Published: 31 May 2020

Abstract: Removal of highly toxic H_2S for pollution control and operational safety is a pressing need. For this purpose, a montmorillonite intercalated with Cu(II)-phenanthroline complex $[Cu[(Phen)(H_2O)_2]^{2+}$ (Mt-CuPhen) was prepared to capture gaseous H_2S under mild conditions. This hybrid material was simple to obtain and demonstrated an outstanding ability to entrap H_2S at room temperature, retaining high efficiency for a very long time (up to 36.8 g of S/100 g Mt-CuPhen after 3 months of exposure). Sorbent and H_2S uptake were investigated by elemental analysis, X-ray powder diffraction measurements, diffuse reflectance (DR) UV–Vis and infrared spectroscopy, thermal analysis and evolved gas mass spectrometry, scanning electron microscopy equipped with energy-dispersive X-ray spectrometer, and X-ray absorption spectroscopy. The H_2S capture was studied over time and a mechanism of action was proposed. The entrapping involves a catalytic mechanism in which $[Cu[(Phen)(H_2O)_2]^{2+}$ acts as catalyst for H_2S oxidation to S^0 by atmospheric oxygen. The low cost and the long-lasting performance for H_2S removal render Mt-CuPhen an extremely appealing trap for H_2S removal and a promising material for many technological applications.

Keywords: layer silicates; clay minerals; montmorillonite; copper; hydrogen sulfide; catalytic oxidation; intercalation; gas trapping

1. Introduction

Expandable layered aluminosilicate minerals, due to properties such as surface acidity, particle size and shape, high surface area, ion exchange, hydration, swelling, plasticity, rheological behavior, and reactivity towards organic and inorganic compounds, are widely used for many industrial applications as sorbents, catalysts, ion-exchangers, additives [1,2]. Among the various layered aluminosilicates, montmorillonite (Mt,), which is a 2:1 dioctahedral smectite [1], received great attention because of its

surface properties, swelling, and ion exchange features that can be further enhanced by exchanging natural inorganic cations in the interlayer space (mostly Ca^{2+} and Na^{+}) with other organic or inorganic species [3–5]. Because of their unique structure, low cost, natural abundance, and environment friendliness, both natural and exchanged Mt were proposed as adsorbent materials for removing multiple contaminants from aquatic systems [6], and more recently, also to capture airborne pollutants such as CO_2, SO_2, NO_x, H_2S, and volatile organic compounds (VOCs) [7–12].

Hydrogen sulfide, a common waste product of industrial processes, is a highly toxic, colorless, and smelly pollutant that occurs in several hydrocarbon sources such as natural gas, biogas, and crude oil. H_2S is harmful to animals and human beings, and is also dangerous to industrial facilities in the gaseous form or in solution. Combustion of fuels containing H_2S releases toxic sulfur oxides into the atmosphere that yield acid rain by reaction with water molecules. Therefore, removal of industrially derived H_2S for pollution control and operational safety is a pressing need. To remove H_2S effectively, several approaches were developed, such as adsorption, scrubbing, hydrodesulfurization, biological treatment, and catalytic oxidation [13].

Recently, porous materials (e.g., activated carbon, porous metal oxides, mesoporous silica, metal-organic and zeolite-like frameworks) with high sulfur removal capacity and selectivity, thermal durability, and good reproducibility attracted great attention for use in H_2S adsorptive removal processes, particularly at low temperature, as they grant cost-effective approaches with deep H_2S removal [13]. Usually the surface of these porous materials is functionalized with organic or inorganic functional groups to enhance and/or modify physical and chemical surface properties and reactivity. Amine grafting, heteroatom (nitrogen) doping, alkaline impregnation, and metal oxide incorporation are the most widely applied approaches for the surface functionalization of these porous structures [13].

Layered aluminosilicate microporous structures, such as pillared clays doped with metallic cations (usually Fe^{3+}, Zn^{2+}, and Cu^{2+}) and/or clays intercalated with metal–organic functional groups were also tested for selective catalytic oxidation of H_2S [13]. Recent studies dealing with the removal of sulfur gaseous compounds by means of different types of metal–organic functionalized Mt demonstrated that this mineral intercalated with Fe(III)-phenanthroline complex is one of the best performing materials [9,14]. The H_2S trapping process involves a redox reaction between Fe^{3+} and a first S^{2-} ion, followed by the binding of a second S^{2-} ion to the metal center. It occurs at room temperature, is reversible, and does not require pretreatment [14].

Based on these premises, these materials deserve further investigation to explore new possible applications and developments. In this work, we studied the adsorption mechanism of H_2S by montmorillonite intercalated with a Cu(II)-phenanthroline complex (Cu(II)Phen). Cu oxides are commonly used to catalytically oxidize adsorbed H_2S gas, thus suggesting that H_2S trapping efficiency of Mt intercalated with cation-phenanthroline complexes can be improved by employing copper instead of iron.

2. Materials and Methods

2.1. Preparation of H_2S Sorbent Material

Montmorillonite STx-1b from Gonzales County (Monthalia, TX, USA) (Mt, for all other abbreviations see Appendix A) was obtained from the Source Clay Repository of the Clay Minerals Society. Mt was already fully characterized elsewhere [15]. Its main characteristics are briefly summarized: mineralogical composition, obtained from quantitative X-ray powder diffraction results (QXRDP), montmorillonite 73%, cristobalite 12.8%, tridymite 11.6%, quartz 0.12%, amorphous 2%; chemical formula, obtained by combining chemical data and QXRDP results, $(Si_{7.753}Al_{0.247})(Al_{3.281}Mg_{0.558}Fe_{0.136}Ti_{0.024}Mn_{0.002})(Ca_{0.341}Na_{0.039}K_{0.061})O_{20}(OH)_4$; cation exchange capacity (CEC) 66.1 ± 2.1 meq/100 g. It was used as received, without further purification.

The H_2S-sorbent material was obtained by exchanging Mt with a solution of a Cu(II)-phenanthroline complex, $[Cu[(Phen)(H_2O)_2]^{2+}$ (hereafter Cu(II)Phen).

The same chemicals and procedures described by the authors in a previous study were used [11]. Specifically, $CuSO_4 \cdot 5H_2O$ was dissolved at room temperature in a well-stirred phenanthroline (Phen) solution in order to obtain a 6 mM solution of Cu(II)Phen; Mt (50 mg) was dispersed in 10 mL of this solution, shaken for 1 h at 250 rpm at room temperature, and then separated from the liquid phase via centrifugation at 14,000× *g* for 1 min. The final powder was washed several times with distilled water and then dried at 30 °C overnight. The resulting material, Mt-CuPhen, contains large amounts of Cu ions in the interlayer, 0.651 Cu^{2+} moles/kg. An extensive characterization of Mt-CuPhen material was described in detail elsewhere [11].

2.2. Exposure of Mt-CuPhen to H_2S Gas Stream

The reaction tests were carried out in a continuous flow reactor made with a glass box covered by layer of aluminum foil, hosting an inner and outer gas hose. One hundred mg of Mt-CuPhen were dispersed on the bottom of the glass box. A mixture of H_2S/air (samples exposed in aerobic conditions) and H_2S/Ar (samples exposed in anaerobic conditions) was fluxed into the box at a constant H_2S partial pressure of 250 Pa, controlled by calibrated mass flow controllers (Alltech Digital Flow Check-HR) and gas mixing valves. H_2S adsorption tests were completed at different times (up to 3 months). The S content of Mt-CuPhen samples exposed to H_2S (Mt-CuPhen-exp H_2S) was determined by elemental analysis; measurements were repeated three times to obtain mean values with a statistical significance.

2.3. Characterization of Mt-CuPhen Exposed to H_2S Gas Stream

The elemental analyses (C, N, and S) were performed using a Carlo Erba 1106 Elemental Analyzer. UV–Vis and diffuse–reflectance (DR) UV–Vis analyses were carried out by the Jasco V-570 Instrument equipped with an integrating sphere attachment (JASCO model ISN-470) to analyze the powder samples. $BaSO_4$ was used as reference. X-ray powder diffraction (XRPD) measurements were performed by an analytical X'Pert PRO powder diffractometer equipped with an X'Celerator detector on standard glass slides in the 2–50° 2θ range. Analytical conditions were: incident beam, Cu *K*α radiation (λ = 1.54184 Å) at 40 kV and 40 mA (nickel filtered); Soller slits, 0.04 rad; antiscatter mask, 20 mm; antiscatter slit, 1/4°; divergence slit, 1/4°. Diffracted beam: antiscatter mask, 5.0 mm; Soller slits, 0.04 rad; integration time, 30 s in continuous scanning (PSD length of 2.12° 2θ corresponding to a step size of 0.0170° 2θ per s). Quartz was used as calibration standard.

IR spectra (4000–400 cm^{-1}) were recorded by a JASCO FT/IR 4700 spectrophotometer (resolution: 0.4 cm^{-1}) with KBr used as the dispersing medium.

The morphology and elemental composition of samples were characterized by scanning electron microscopy (SEM) by using an FEI Quanta 200 ESEM and an energy-dispersive X-ray spectrometer attached to the Quanta 200 ESEM (X-EDS Oxford INCA-350 system EDX).

A Seiko SSC 5200 thermal analyzer equipped with a quadrupole mass spectrometer (ESS, GeneSysQuadstar 422) was employed in the thermal studies. The powdered samples (10 mg) were heated from 25 to 1050 °C in helium flowing. Gas analyses were carried out in multiple ion detection mode (MID) and different m/z ratios were considered (17 and 18 for H_2O; 28 and 44 for CO_2; 30 for NO and NO_2; 33 and 34 for H_2S; 46 for NO_2; 48, 64, and 66 for SO_2). Experimental conditions were: heating rate = 10°/min; heating range = 25–1050 °C; data measurement = every 0.5 s; purging gas = ultrapure helium, flow rate = 100 μL/min. Before starting measurements, samples were equilibrated for 15 min using a 100 μL/min flow of ultrapure helium [14].

X-ray absorption spectroscopy (XAS) spectra were measured at the Spanish CRG beamline BM25-Spline at the European Synchrotron Radiation Facility (ESRF), Grenoble (France). XAS spectra were collected at the Cu *K*-edge (8979 eV) in both transmission and fluorescence mode at room temperature on pellets prepared by mixing uniformly the powered samples and cellulose. The fluorescence signal was collected using a nitrogen cooled 13-element Si (Li) solid state detector (e2v Scientific Instruments) located at 90° with respect to the incoming X-ray beam, while the transmitted photons were measured with an ionization chamber gas-filled with 50% N_2 and 50% Ar. The incident

beam intensity was also monitored by using an ionization chamber with 100% N_2. For all spectra, a metallic Cu foil was employed to provide an energy calibration for the monochromator. As reference materials, pure Cu_2O, CuO, CuS, $CuSO_4{\cdot}5H_2O$, and $Cu_3(CO_3)_2(OH)_2$ compounds were used. The XAS spectra were recorded over a wide energy range across the Cu *K*-absorption edge with 0.25 eV energy step in the X-ray absorption near-edge structure (XANES) region and 0.04 $Å^{-1}$ in the extended X-ray absorption fine structure (EXAFS) region up to 15 $Å^{-1}$. The X-ray absorption data were analyzed with a standard procedure using ATHENA software [16].

3. Results and Discussion

3.1. H_2S Capture by Mt-CuPhen

The S amounts measured by elemental analysis on Mt-CuPhen exposed to H_2S vapors for different times are plotted in Figure 1. Mt-CuPhen captures a great amount of sulfur (up to 1.15 S moles/100 g Mt-CuPhen after 3 months of exposure) and its immobilization ability lasts for a very long time.

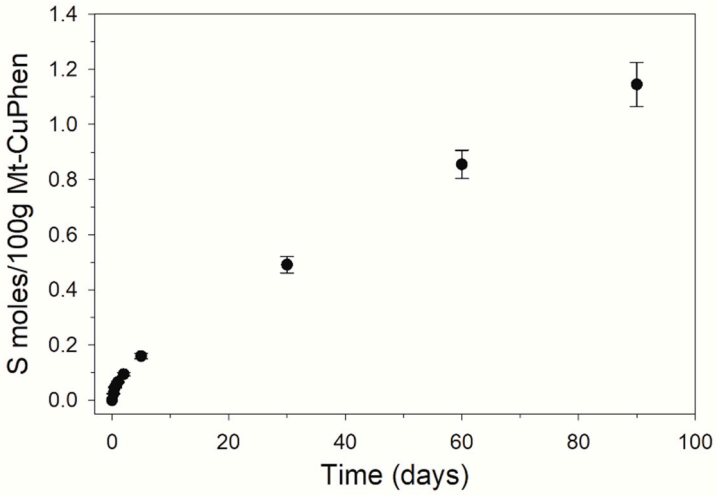

Figure 1. Plot of S content from H_2S (the S content due to sulfate anions in the starting Mt-CuPhen was subtracted) in Mt-CuPhen as a function of the time of exposure to H_2S. Error bars indicate the variability of each measure.

The H_2S capture proceeds without reaching completion, following a pathway that differs from that reported for Mt intercalated with the μ-oxo binuclear Fe(III)-phenanthroline 1:1 complex ($[(H_2O)_3PhenFe\text{-}O\text{-}FePhen(H_2O)_3]^{4+}$, FePhen hereafter) [14]. For the latter, the H_2S removal process occurs into two distinct steps: the former, lasting for about 20 h, is fast in the first 4 h and then slows down, while the latter is completed within about 110 h. Overall, the process lasts 110 h; eventually the exhaust material must be regenerated by a thermal treatment at 295 °C for reuse.

The larger maximum amount of S captured by Mt-CuPhen compared to Mt-FePhen (up to 1.15 moles (36.8 g) of S/100 g vs. 0.12 moles (3.8 g) of S/100 g, respectively) and the longer uptime of the material indicate a radical change in the entrapping mechanism [14].

3.2. DR UV–Vis Spectra

The diffuse–reflectance (DR) UV–Vis spectra of Mt-CuPhen in the range $200 \leq \lambda \leq 1000$ nm before and after exposure to H_2S are shown in Figure 2. As described previously [11], when compared to Mt, Mt-CuPhen shows: (i) the appearance of a signal at $\lambda = 270$ nm corresponding to the overlap of Mt ($\lambda = 256$ nm) and Cu(II)Phen ($\lambda = 272$ nm) signals; (ii) a band at $\lambda = 300$ nm ($\pi \rightarrow \pi^*$ transition of phenanthroline bond to Cu^{2+}); (iii) three shoulders at $\lambda = 316$, 332, and 350 nm (related to phenanthroline transitions); (iv) a large band at about $\lambda = 780$ nm, due to Cu^{2+} d → d transition); and (v) a band at

λ = 920 nm, most likely associated to H_2O molecules (overtone) related to Cu^{2+}, due to the adsorbed Cu(II)Phen.

When Mt-CuPhen is exposed to H_2S, its spectrum changes dramatically (Figure 2). A well-defined shoulder at about λ = 520 nm appears, while the absorption band at λ = 780 nm drops down. Both bands, however, coexist in the spectra recorded at different exposure times (from 10 min to three months), although a change in the absorbance ratio occurs. The new band at λ = 520 nm can be confidently attributed to Cu(I)Phen complexes, suggesting that the capture of H_2S involves a Cu(II) reduction step. The spectra are very similar to those for Cu(II)Phen intercalated in Mt reduced with ascorbic acid and then exposed to heptanethiol vapors. In addition, for this case, an absorption band related to Cu(I)Phen-thiolate complex appears at about 530 nm [17,18]. Likewise, the profiles of the DR UV–Vis spectra previously obtained for Mt-FePhen exposed to H_2S gaseous streams show an intensity decrease for the band at λ = 374 nm, attributed O^{2-}(bridge) → Fe(III) charge-transfer transition, typical of the μ-oxo ferric complexes, together with a concomitant increase in the band at λ = 520 nm, due to a d → π* metal-to-ligand charge transfer of $[Fe(II)Phen]^{2+}$ type complex, suggesting a Fe(III) to Fe(II) reduction [14].

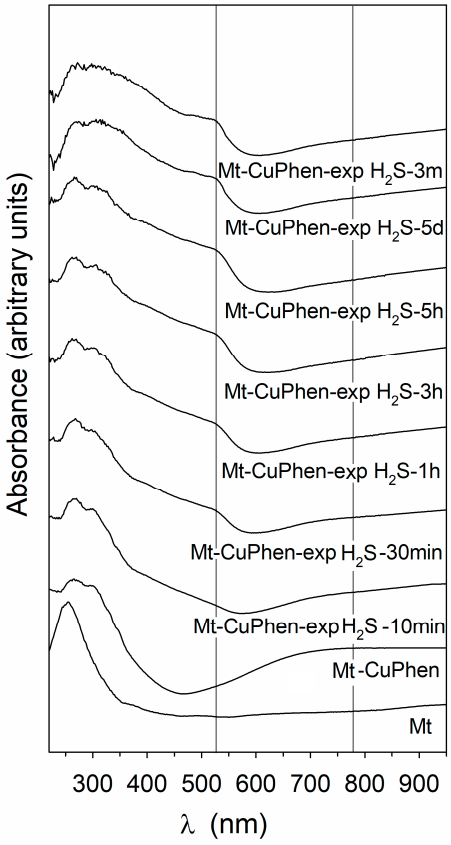

Figure 2. Diffuse–reflectance (DR) UV–Vis spectra of Mt-CuPhen and of Mt-CuPhen exposed to H_2S for different times. Curves were shifted on the y-axis for sake of clarity. Lines at λ = 520 nm and λ = 780 nm mark features discussed in the text.

3.3. Scanning Electron Microscopy (SEM) and Energy Dispersive X-ray Spectrometry (EDX)

SEM images (Figure 3) show the formation on the Mt surface of crystals with a size of about 5–10 μm (Figure 3a) and about 10–50 μm (Figure 3b) for Mt-CuPhen exposed to H_2S for 3 days and 3 months, respectively. The polyhedral shape of the crystals becomes well defined and the size increases with increasing the exposure time. As shown by EDX, these crystals are mainly constituted by elemental S; minor signals related to Al and Si are probably due to the Mt substrate. Therefore, the final product of the interaction of Mt-CuPhen with H_2S is well-crystallized sulfur.

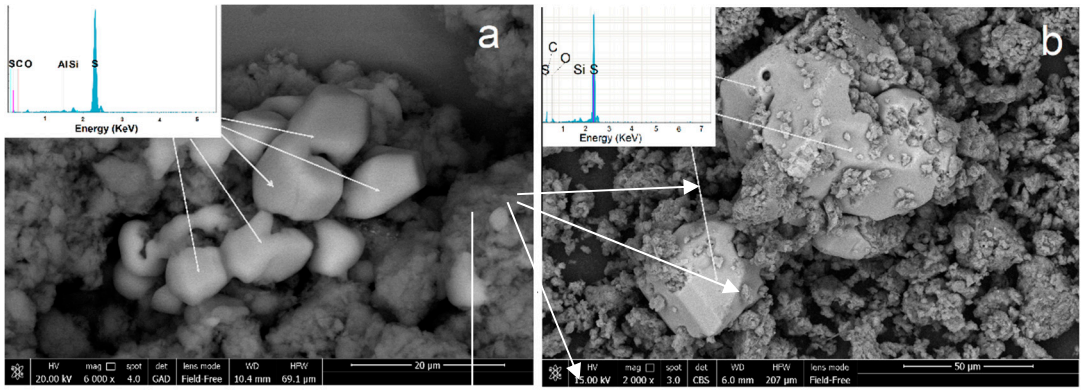

Figure 3. Scanning electron microscopy (SEM) images of Mt-CuPhen exposed to H_2S for different times: (**a**) 3 days; (**b**) 3 months. The energy dispersive X-ray spectrometry (EDX) spectra reported refer to crystals indicated by arrows.

3.4. X-ray Diffraction (XRPD)

XRPD analysis was carried out on Mt-CuPhen samples before and after a three-month exposure to H_2S in order to better recognize the sulfur phase.

The XRPD patterns ($3 \leq 2\theta(°) \leq 40$) of Mt-CuPhen before and after exposure are shown in Figure 4. As discussed previously [11,15], the diffraction peaks of Mt-CuPhen with respect to Mt show: (i) a shift towards higher d values of d_{001} reflection (d_{001} Mt = 1.51 nm; d_{001} Mt-CuPhen = 1.71 nm), suggesting that CuPhen species coordinated by sulfate groups, which are about 0.71 nm thick, that occupy the interlayer positions; (ii) higher order XRD reflections, which are approximate multiples of the 2θ angle of the 001 reflection [19], suggesting the presence of more ordered domains.

The exposure of Mt-CuPhen to H_2S does not affect the Mt-CuPhen d_{001}-spacing. The d_{001} peak position is always at 1.71 nm. However, some additional peaks (e.g., at 0.6040, 0.3816, 0.3429, 0.3337 nm) were recognized, which can all be related to rosickyite (i.e., monoclinic sulfur), as evaluated by means of the PANalytical X'Pert HighScore software and the ICDD PDF-2 database. These results agree with the outcome of the SEM/EDX analysis, namely that the final reaction product of the interaction between Mt-CuPhen and H_2S gas is crystalline sulfur.

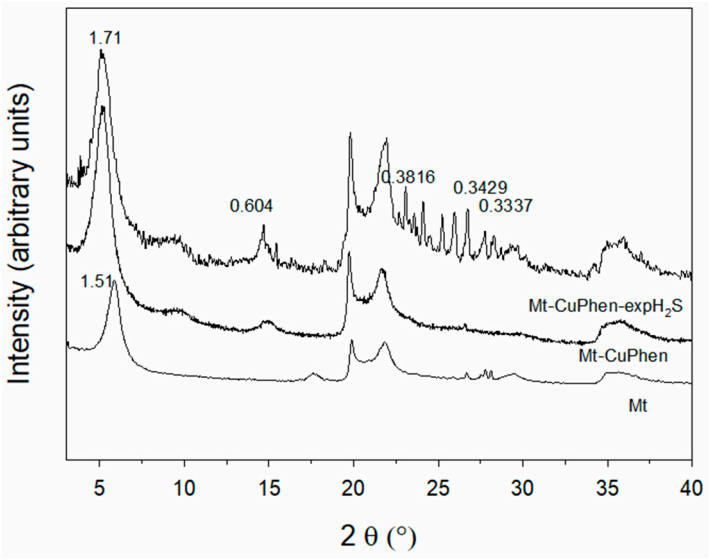

Figure 4. X-ray diffraction patterns of Mt and Mt-CuPhen before and after exposure to H_2S. Numbers on peaks indicate the d_{hkl} values (nm).

3.5. FTIR Spectra

To expand the depth of our analysis of the mechanism of hydrogen sulfide immobilization, FTIR spectra for Mt-CuPhen before and after exposure to H_2S were recorded (Figure 5). The two samples showed the typical spectrum of montmorillonite-based material, namely an absorption band centered at 3626 cm^{-1} for Mt-CuPhen and 3620 cm^{-1} for Mt-CuPhen-exp H_2S-3m due to the stretching vibration of octahedral OH, a broad band centered at about 3435 cm^{-1}, due to νOH modes of H_2O, a band at 1630 cm^{-1} (δH_2O for water bending vibration), at 1086 and 1042 cm^{-1} (Si(Al)-O bonds stretching), and between 700 and 950 cm^{-1} (structural OH-bending mode) [15].

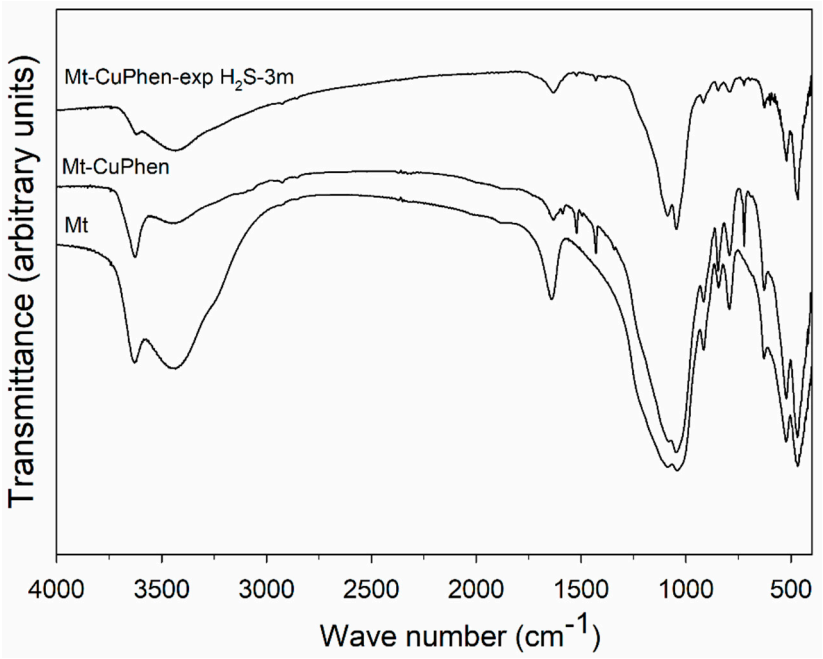

Figure 5. FTIR spectra for Mt-CuPhen before and after exposure to H_2S for 3 months (Mt-CuPhen-exp H_2S-3m). The Mt spectrum was also introduced as reported by Castellini et al. [15].

Additional bands typical of Cu(II)Phen between 3000 and 3200 cm^{-1} (aromatic ring C-H stretching), at 1588, 1522, 1495, and 1429 cm^{-1} (C–C and C–N stretching of the Phen ring) and at 722 cm^{-1} (C–H out-of-plane bending of heterocyclic ring) are also evident [14].

The comparison of Mt-CuPhen spectra before and after exposure to H_2S shows very few differences. In particular, no S–H stretching vibration characteristic of H_2S is observed between 2500 and 2625 cm^{-1} in the Mt-CuPhen-exp H_2S-3m spectrum, indicating the absence of any physisorbed H_2S (Figure 5) [20]. Of note, elemental sulfur cannot be detected with FTIR because of the absence of a distinct signature. In addition, the bands at around 1415 and 1380 cm^{-1}, indicative of sulfate ions, are not evidenced in the Mt-CuPhen-exp H_2S-3m spectrum [14,21,22].

In both samples, changes in the bands related to ν(OH) and δH_2O of water molecules, clearly visible in Mt, are observed. In particular, an intensity decrease occurs in the sample not exposed to H_2S.

3.6. Thermal Analysis of Mt-CuPhen before and after Exposure to H_2S

Thermogravimetric analyses (TGA), their first derivative signals (DTGA), and mass spectrometry curves of gases evolved during heating (m/z = 18 and m/z = 64) of Mt-CuPhen and Mt-CuPhen-exp H_2S-25d are plotted in Figures 6 and 7.

Attention was focused on the reactions occurring in the temperature range 25 °C ≤ T ≤ 400 °C as most of the effects related to this study occurs in this range. At higher temperature, thermal tracings of Mt-CuPhen-exp H_2S-25d are similar to those obtained for Mt-CuPhen discussed previously [11,18].

TGA curves of Mt-CuPhen, before and after H_2S exposure, show a mass loss (Δm%) associated with a broad peak in DTGA tracing at about 80 °C (Δm% Mt-CuPhen = 3.32; Δm% Mt-CuPhen-exp H_2S-25d = 3.63; Figure 6). For both samples the mass loss related to this effect, linked to the loss of outer-sphere H_2O (m/z = 18, Figure 7), is lower compared to Mt (Δm% in pristine Mt = 10.6) [15]. The thermal effect at about 150 °C, that in untreated Mt is associated to the loss of inner-sphere H_2O, completely disappears. The amount of water in the sample exposed to H_2S is slightly larger than that prior to exposure (Figure 7), in agreement with the FTIR data.

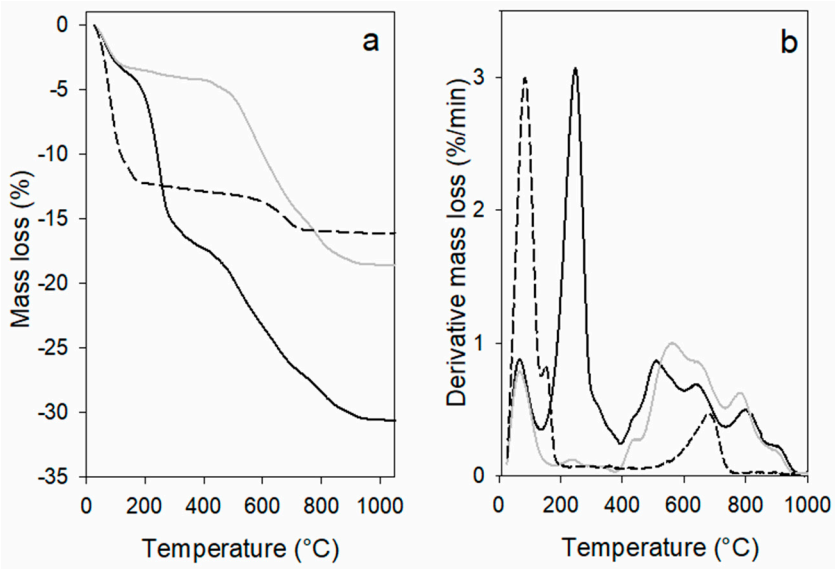

Figure 6. Thermal analyses of Mt (black dashed lines), Mt-CuPhen (solid gray line) and Mt-CuPhen-exp H_2S-25d (black solid lines). (**a**) Thermogravimetric analysis tracings (TGA), (**b**) corresponding derivative signals of thermogravimetric curves (DTGA).

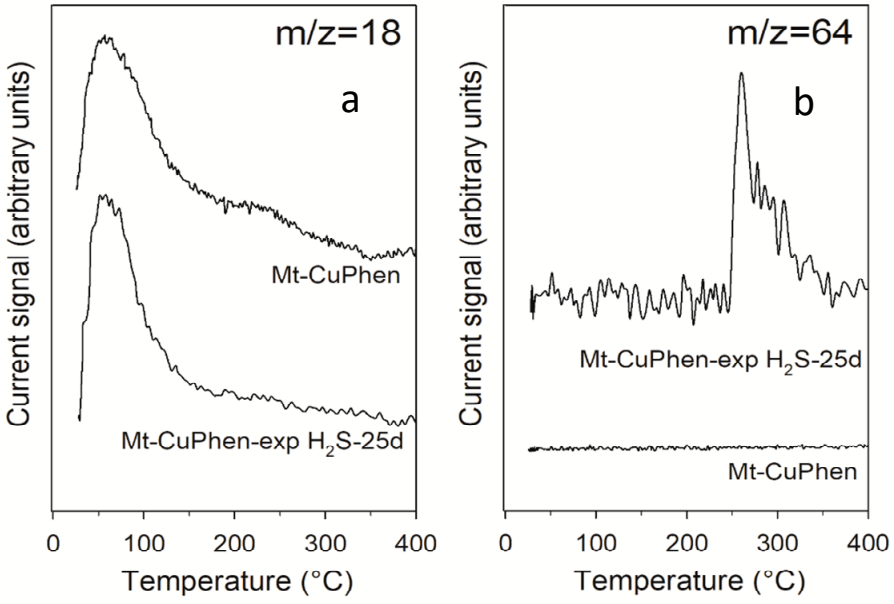

Figure 7. Tracings of gas evolved during heating for Mt-CuPhen before and after H_2S exposure (25 d) for H_2O (**a**) (m/z = 18) and SO_2 (**b**) (m/z = 64).

A second large mass loss (Δm% = 13.10) is observed for Mt-CuPhen-exp H_2S-25d sample between 160 and 360 °C and is associated to a strong effect centered at 235° in DTG tracing. This mass loss can be confidently attributed to the oxidation of elemental sulfur also observed by SEM/EDX and

XRPD analyses. Accordingly, an associated release of SO_2 was detected by mass analysis (Figure 7, m/z = 64). Pure H_2S is not significantly adsorbed by Mt-CuPhen, since its release should be observed at temperatures lower than 120 °C [20,21].

3.7. XAS Analysis of Mt-CuPhen before and after H_2S Exposure

The XANES study at the Cu *K*-edge of Mt-CuPhen before and after H_2S exposure under different conditions was carried out to gain information on the Cu oxidation state, coordination symmetry, and electronic structure. XANES spectra of Mt-CuPhen and reference compounds are reported in Figure S1 and strictly resemble those already reported and discussed elsewhere [18].

In Figure S1a, Cu reference compounds with formal 2+ oxidation state display different position, intensity, and shape of the absorption edge, which can be attributed to the different nature of the ligand and to Cu local geometry [23–27]. Changes also occur for the Cu(II)Phen crystals and Mt-CuPhen material (Figure S1b). The reference compounds CuO and $CuSO_4{\cdot}5H_2O$, both containing Cu(II), show differences in the XANES region that can be attributed to the different Cu coordination (i.e., square planar geometry for CuO and octahedral geometry for $CuSO_4{\cdot}5H_2O$) [26]. The XANES profile of Cu(II)Phen crystals (Figure S1b) is closer to that of $CuSO_4{\cdot}5H_2O$; however, it shows a pre-edge of low intensity, an absorption edge moved to higher energy with respect to $CuSO_4{\cdot}5H_2O$, and a whiteline of high intensity. These features indicate that a certain distortion of the octahedral coordination of Cu(II) center occurs [11,18]. The XANES signal of Mt-CuPhen is still similar to that for Cu(II)Phen crystals, but show clear intermediate characteristics between CuO and Cu(II)Phen, probably due to an even more pronounced distortion of the octahedral coordination of Cu(II) or even a decrease in its coordination number (possibly from six to five, thus assuming a square pyramidal geometry) [26]. Figure S2 shows the evolution of Mt-CuPhen XANES spectrum at different H_2S exposure times. After 12 h exposure to H_2S vapors (Mt-CuPhen-exp H_2S-12h), a shift of the absorption edge towards lower energies occurs, consistent with a reduction of Cu(II) to Cu(I) and a decrease of both peak intensity at the absorption edge (around 8982 eV) and of the whiteline (around 8997 eV). These features are also evident in XANES spectrum obtained on the sample exposed for 5 days to H_2S (Mt-CuPhen-exp H_2S-5d), afterwards the modifications of the XANES signal are slight and within the measurement resolution. The XANES signals of Mt-CuPhen samples exposed to H_2S under anaerobic conditions (samples Mt-CuPhen-exp H_2S ac-12h and Mt-CuPhen-exp H_2S ac-1m) are closer to those of the Cu_2O reference, displaying a larger shift of the absorption edge towards lower energies and a decrease in the intensity of peaks around 8982 and 8997 eV with respect to what observed in aerobic conditions, thus suggesting a large reduction of the average Cu oxidation state (Figure S2b).

Mt-CuPhen exposed to H_2S for 1 month in anaerobic conditions and then exposed to air for 2 weeks (sample Mt-CuPhen-exp H_2S ac-1m-air) shows XANES features close to that of Mt-CuPhen exposed to H_2S for 12 h in both anaerobic and nonanaerobic conditions. The position of absorption edge falls at higher energy compared to Mt-CuPhen-exp H_2S ac-1m indicating the reoxidation of copper ion after the exposure to air.

As observed for the K edge of transition metals, the absorption edge position of XANES spectra shifts with the average copper oxidation state. Thus, in order to evaluate semiquantitatively the coexistence of Cu(II) and Cu(I) atoms when Mt-CuPhen is exposed to H_2S gas, the correlation known as Kunzl's law was applied [28,29]. The linear relationship:

$$E_e = 8978\ (3) + 3\ (1)\ OS \quad (1)$$

correlating the position of the absorption edge (E_e) with the mean oxidation state (*OS*) was evaluated from the peak position of reference compounds. The results confirm that the Cu(II)Phen crystals and Mt-CuPhen contain Cu(II) ion (calculated oxidation state: 2.3 ± 0.3, Figure S3a). After 12 h exposure to H_2S gas, the average oxidation state of Cu in Mt-CuPhen decreases to 1.3 ± 0.3, indicating partial Cu(II)

reduction to Cu(I). For larger exposure times, the average oxidation state of Cu increases (1.5 ± 0.3 for 5 days and 2.0 ± 0.3 for exposure times higher than 1 month).

The average oxidation state of samples exposed to H_2S under anaerobic conditions was also calculated (Figure S3b). The sample exposed for 12 h shows an average oxidation state (1.3 ± 0.3) similar to that of the material exposed under aerobic conditions (1.3 ± 0.3), but upon increasing exposure times Cu is found almost entirely in the reduced state (after 1 month the average oxidation state is 1.1 ± 0.3 and 2.0 ± 0.3 under anaerobic and aerobic conditions, respectively). The reversibility of the reduction process is confirmed by the sharp change of the oxidation state of the sample exposed anaerobically to H_2S by simple eventual exposure to air (after two weeks the average oxidation state varies from 1.1 to 1.8).

3.8. Catalytic Mechanism Responsible for Oxidation of H_2S to S^0

H_2S capture by Mt-CuPhen reasonably occurs with a multistep process. Spectroscopic data (DR UV–Vis and XANES spectra) indicate that Cu(II)Phen intercalated in Mt undergoes reduction to Cu(I)Phen when exposed to H_2S. This reaction is coupled to the oxidation of S^{2-} to S^0, as shown by the presence of sulfur crystals (XRPD and SEM measurements). S^0 is produced in a molar amount much larger than that of Cu(II) present in Mt-CuPhen (after 3 months S/Cu molar ratio = 17.7). Moreover, Cu(II) and Cu(I) always coexist during the formation of S° even at very long exposure times. This indicates a catalytic process for oxidation of sulfide involving atmospheric oxygen. Based on the above results, a tentative reaction mechanism can be proposed:

$$2\,[\text{Cu(II)Phen}]^{2+} + 2\,H_2S \rightarrow S^0 + [\text{PhenCu(I)-S-Cu(I)Phen}] + 4H^+ \quad (2)$$

$$[\text{PhenCu(I)-S-Cu(I)Phen}] + 4H^+ + O_2 \rightarrow 2\,[\text{Cu(II)Phen}]^{2+} + S^0 + 2\,H_2O \quad (3)$$

In such a way, $[\text{Cu(II)Phen}]^{2+}$ acts as a catalyst and makes the reaction proceed cyclically leading to the formation of elemental sulfur from H_2S, the overall reaction being:

$$2\,H_2S + O_2 \rightarrow 2\,S^0 + 2\,H_2O \quad (4)$$

This mechanism accounts for the remarkable difference observed in the immobilization efficiency of Mt-CuPhen with respect to Mt-FePhen. In fact, the oxidation of H_2S by O_2 catalyzed by Mt-CuPhen allows immobilization of larger amounts of sulfur than those obtained with Mt-FePhen, whose entrapping process is based on the direct oxidation of H_2S by Fe(III)Phen without the involvement of any catalytic steps and thus depending only on Fe(III) amount intercalated in Mt.

Mt-CuPhen works for a long time, but at the end of the process it cannot be easily regenerated since the resulting elemental sulfur is largely dispersed and settled on the material.

4. Conclusions

Our study reveals the high efficiency in H_2S trapping of montmorillonite intercalated with Cu-phenanthroline complex. The replacement of FePhen with CuPhen allows for achieving the capture of H_2S through a catalytic mechanism that substantially changes both the quantity of this gas that can be immobilized and the duration of the uptake process. Mt-CuPhen offers a promising performance towards gaseous H_2S removal because its immobilization ability is very high, displays a long-time duration (36.8 g of S/100 g Mt-CuPhen after 3 months of exposure) and works at low (room) temperature conditions. Thus, this material provides a long-term stability and complies with the request to lower the operational costs in industrial applications.

Although the formation of sulfur crystals as final product compromises the thermal regeneration of Mt-CuPhen, the low cost of the starting material and the long-lasting adsorption performances (more than 3 months), make the process cost effective and promising for technological applications. Therefore, it is a sound alternative to montmorillonite treated with Fe(III)-phenanthroline complex. In

fact, the latter, while being renewable by thermal treatment, is less effective in H_2S trapping and needs to be replaced or renewed much more often.

Supplementary Materials: The following are available online at http://www.mdpi.com/2075-163X/10/6/510/s1, Figure S1: (a) XANES spectra of Cu(II)Phen crystals and Mt-CuPhen compared with the spectra of several reference compounds: Cu_2O, CuO, CuS, $CuSO_4{\cdot}5H_2O$, and $Cu_3(CO_3)_2(OH)_2$. (b) XANES spectra of Cu(II)Phen crystals and Mt-CuPhen compared with the CuO and $CuSO_4{\cdot}5H_2O$ references showing more clearly the XANES features of compounds. (c) Smoothed first derivative of absorption signal of Cu(II)Phen crystals, Mt-CuPhen and reference compounds; Figure S2: XANES spectra of Mt-CuPhen exposed to H_2S gas under different conditions. (a) Mt-CuPhen exposed to H_2S for different times, i.e., 12 h, 5 days, 1 month, 2 months, and (b) Mt-CuPhen exposed 12 h and 1 month to H_2S in aerobic and anaerobic conditions and Mt-CuPhen first exposed to H_2S for 1 month in anaerobic conditions and then exposed to air for 2 weeks; Figure S3: Linear relationship between position at Cu *K*-absorption edge and the oxidation state for reference compounds, Cu(II)Phen crystals, Mt-CuPhen material and this last one exposed to H_2S gas under different conditions: (a) Mt-CuPhen exposed to H_2S for 12 h (Mt-CuPhen-exp H_2S-12h), 5 days (Mt-CuPhen-exp H_2S-5d), 1 month (Mt-CuPhen-exp H_2S-1m), 2 months (Mt-CuPhen-exp H_2S-2m) in aerobic conditions, (b) Mt-CuPhen exposed to H_2S in anaerobic conditions for 12 h (Mt-CuPhen-exp H_2S ac-12h), 1 month (Mt-CuPhen-exp H_2S ac-1m), and for 1 month and re-exposed to air (Mt-CuPhen-exp H_2S ac-1m-air).

Author Contributions: Conceptualization, E.C. and M.F.B.; methodology, C.I.S.-D., G.R.C., D.M., and M.B.; validation, C.I.S.-D., G.R.C., and D.M.; formal analysis, F.B., L.S., A.S.; investigation, F.B., L.S., and A.S.; data curation, L.S. and A.S.; writing—original draft preparation, E.C. and M.F.B.; writing—review and editing, E.C. and M.F.B.; supervision, M.B.; project administration, E.C. and M.B.; funding acquisition, D.M. and A.S. All authors have read and agreed to the published version of the manuscript.

Funding: This research is under the contribution of Ministero dell'Università e della Ricerca (MIUR), PRIN2017 project "Mineral Reactivity, a Key to Understand Large-Scale Processes: from Rock Forming Environments to Solid Waste Recovering/Lithification"—Project Code 2017L83S77. A.S. acknowledges financial support from the Ministerio Español de Ciencia, Innovación y Universidades (MCIU) through the project RTI2018-095303-A-C52 and the Comunidad de Madrid for an "Atracción de Talento Investigador" contract (No. 2017-t2/IND5395).

Acknowledgments: The European Synchrotron (ESRF), MCIU and Consejo Superior de Investigaciones Cientificas (CSIC) are acknowledged for the provision of synchrotron radiation facilities. We also thank the BM25-SpLine staff and CIGS (University of Modena and Reggio Emilia) for the technical support.

Conflicts of Interest: The authors declare no conflict of interest.

Appendix A

Table A1. The list of abbreviations.

Phen	1,10-phenanthroline
Cu(II)Phen	$[Cu[(Phen)(H_2O)_2]^{2+}$
Mt-CuPhen	solid hybrid material obtained by Mt treated with Cu(II)Phen complex
Mt-CuPhen-exp H_2S-10min	Mt-CuPhen exposed to H_2S vapor for 10 min
Mt-CuPhen-exp H_2S-30min	Mt-CuPhen exposed to H_2S vapor for 30 min
Mt-CuPhen-exp H_2S-12h	Mt-CuPhen exposed to H_2S vapor for 12 h
Mt-CuPhen-exp H_2S-5d	Mt-CuPhen exposed to H_2S vapor for 5 days
Mt-CuPhen-exp H_2S-25d	Mt-CuPhen exposed to H_2S vapor for 25 days
Mt-CuPhen-exp H_2S-1m	Mt-CuPhen exposed to H_2S vapor for 1 month
Mt-CuPhen-exp H_2S-2m	Mt-CuPhen exposed to H_2S vapor for 2 months
Mt-CuPhen-exp H_2S-3m	Mt-CuPhen exposed to H_2S vapor for 3 months
Mt-CuPhen-exp H_2S ac-12h	Mt-CuPhen exposed to H_2S vapor for 12 h in anaerobic conditions
Mt-CuPhen-exp H_2S ac-1m	Mt-CuPhen exposed to H_2S vapor for 1 month in anaerobic conditions
Mt-CuPhen-exp H_2S ac-1m-air	Mt-CuPhen exposed to H_2S vapor for 1 month in anaerobic conditions and then exposed to air for 2 weeks
Mt-FePhen	solid hybrid material obtained by Mt treated with a μ-oxo 1:1 Fe(III)-phenanthroline complex

References

1. Brigatti, M.F.; Malferrari, D.; Laurora, A.; Elmi, C. Structure and mineralogy of layer silicates: Recent perspectives and new trends. In *Layered Mineral Structures and Their Application in Advanced Technologies*; Brigatti, M.F., Mottana, A., Eds.; European Mineralogical Union and the Mineralogical Society of Great Britain & Ireland, EMU Notes in Mineralogy: London, UK, 2011; Volume 11, pp. 1–71. [CrossRef]
2. Christidis, G.E. Industrial Clays. In *Advances in the Characterization of Industrial Minerals*; Christidis, G.E., Ed.; European Mineralogical Union and the Mineralogical Society of Great Britain & Ireland, EMU Notes in Mineralogy: London, UK, 2009; Volume 9, pp. 341–414. [CrossRef]
3. Bernini, F.; Castellini, E.; Malferrari, D.; Borsari, M.; Brigatti, M.F. Stepwise structuring of the adsorbed layer modulates the physic-chemical properties of hybrid materials from phyllosilicates interacting with the μ-oxo Fe+3 phenanthroline complex. *Microporous Mesoporous Mater.* **2015**, *211*, 19–29. [CrossRef]
4. Baloyi, J.; Ntho, T.; Moma, J. Synthesis and application of pillared clay heterogeneous catalysts for wastewater treatment: A review. *RCS Adv.* **2018**, *8*, 5197–5220. [CrossRef]
5. Castellini, E.; Berthold, C.; Malferrari, D.; Bernini, F. Sodium hexametaphosphate interaction with 2:1 clay minerals illite and montmorillonite. *Appl. Clay Sci.* **2013**, *83–84*, 162–170. [CrossRef]
6. Gu, S.; Kang, X.; Wang, L.; Lichtfouse, E.; Wang, C. Clay mineral adsorbents for heavy metal removal from wastewater: A review. *Environ. Chem. Lett.* **2019**, *17*, 629–654. [CrossRef]
7. Lee, M.S.; McGrail, B.P.; Glezakou, V.A. Microstructural response of variably hydrated Ca-rich montmorillonite to supercritical CO_2. *Environ. Sci. Technol.* **2014**, *48*, 8612–8619. [CrossRef]
8. Cavalcanti, L.P.; Kalantzopoulos, G.N.; Eckert, J.; Knudsen, K.D.; Fossum, J.O. A nano-silicate material with exceptional capacity for CO_2 capture and storage at room temperature. *Sci. Rep.* **2018**, *8*, 11827–11832. [CrossRef]
9. Bernini, F.; Castellini, E.; Malferrari, D.; Castro, G.R.; Sainz Diaz, C.I.; Brigatti, M.F.; Borsari, M. Effective and Selective Trapping of Volatile Organic Sulfur Derivatives by Montmorillonite Intercalated with a μ-oxo Fe(III)−Phenanthroline Complex. *Appl. Mater. Interfaces* **2017**, *9*, 1045–1056. [CrossRef]
10. Castellini, E.; Malferrari, D.; Bernini, F.; Sainz Diaz, C.I.; Mucci, A.; Sola, M.; Brigatti, M.F.; Borsari, M. Trapping at the solid-gas interface: Selective adsorption of naphthalene by montmorillonite intercalated with a Fe(III)-phenanthroline complex. *ACS Omega* **2019**, *4*, 7785–7794. [CrossRef]
11. Castellini, E.; Malferrari, D.; Bernini, F.; Bighi, B.; Mucci, A.; Sainz Diaz, C.I.; Serrano, A.; Castro, G.R.; Brigatti, M.F.; Borsari, M. A new material based on montmorillonite and Cu(II)-phenanthroline complex for effective capture of ammonia from gas phase. *Appl. Clay Sci.* **2019**, *184*, 105386. [CrossRef]
12. Sainz-Díaz, C.I.; Francisco-Márquez, M.; Vivier-Bunge, A. Adsorption of polyaromatic heterocycles on pyrophyllite surface by means of different theoretical approaches. *Environ. Chem.* **2011**, *8*, 429–440. [CrossRef]
13. Khabazipour, M.; Anbia, M. Removal of Hydrogen Sulfide from Gas Streams Using Porous Materials: A Review. *Ind. Eng. Chem. Res.* **2019**, *58*, 22133–22164. [CrossRef]
14. Malferrari, D.; Castellini, E.; Bernini, F.; Serrano Rubio, A.; Castro, G.R.; Sainz Diaz, C.I.; Caleffi, M.; Brigatti, M.F.; Borsari, M. Chemical trapping of gaseous H_2S at high and low partial pressures by an iron complex immobilized inside the montmorillonite interlayer. *Microporous Mesoporous Mater.* **2018**, *265*, 8–17. [CrossRef]
15. Castellini, E.; Bernini, F.; Borsari, M.; Brigatti, M.F.; Castro, G.R.; Malferrari, D.; Medici, L.; Mucci, A. Baseline studies of the Clay Minerals Society Source Clay montmorillonite STx-1b. *Clays Clay Miner.* **2017**, *65*, 220–233. [CrossRef]
16. Ravel, B.; Newville, M. ATHENA, ARTEMIS, HEPHAESTUS: Data analysis for X-ray absorption spectroscopy using IFEFFIT. *J. Synchrotron Radiat.* **2005**, *12*, 537–541. [CrossRef] [PubMed]
17. Kuo, C.H.; Chen, C.H.; Huang, M.H. Seed-Mediated Synthesis of Monodispersed Cu_2O Nanocubes with Five Different Size Ranges from 40 to 420 nm. *Adv. Funct. Mater.* **2007**, *17*, 3773–3780. [CrossRef]
18. Castellini, E.; Malferrari, D.; Bernini, F.; Bighi, B.; Mucci, A.; Sainz Diaz, C.I.; Serrano, A.; Castro, G.R.; Brigatti, M.F.; Borsari, M. Tuning of halobenzenes uptake in montmorillonite from gas phase through a functionalization process involving Cu(II)-phenanthroline and heptanethiol. *Appl. Clay Sci.* **2020**, *192*, 105642. [CrossRef]
19. Moore, D.; Reynolds, R.C., Jr. *X-ray Diffraction and the Identification and Analysis of Clay Minerals*, 2nd ed.; Oxford University Press: New York, NY, USA, 1997; ISBN 9780195087130.

20. Sigot, L.; Ducom, G.; Germain, P. Adsorption of hydrogen sulfide (H2S) on zeolite (Z): Retention mechanism. *Chem. Eng.* **2016**, *287*, 47–53. [CrossRef]
21. Zahid, W.M.; Othman, M.A.; Abasaeed, A.E. Enhanced sulfur removal by a tuned composite structure of Cu, Zn, Fe, and Al elements. *J. Hazard. Mater.* **2017**, *331*, 273–279. [CrossRef]
22. Frost, R.L.; Reddy, B.J.; Keeffe, E.C. Structure of selected basic copper (II) sulphate minerals based upon spectroscopy: Implications for hydrogen bonding. *J. Mol. Struct.* **2010**, *977*, 90–99. [CrossRef]
23. Gaur, A.; Shrivastava, B.D. A comparative study of the methods of speciation using X-ray absorption fine structure. *Acta Phys. Pol. Ser. A* **2011**, *121*, 647–652. [CrossRef]
24. Kim, W.B.; Lee, J.S. Quantitative XANES Analysis of Cuprous Dibromide Complex Formed in the Oxidative Carbonylation of Phenols. *J. Phys. Chem. B* **2003**, *107*, 9195–9202. [CrossRef]
25. Shimizu, K.; Maeshima, H.; Yoshida, H.; Satsuma, A.; Hattori, T. Ligand field effect on the chemical shift in XANES spectra of Cu(II) compounds. *Phys. Chem. Chem. Phys.* **2001**, *3*, 862–866. [CrossRef]
26. Gaur, A.; Klysubun, W.; Nitin Nair, N.; Shrivastava, B.D.; Prasad, J.; Srivastava, K. XAFS study of copper(II) complexes with square planar and square pyramidal coordination geometries. *J. Mol. Struct.* **2016**, *1118*, 212–219. [CrossRef]
27. Giorgetti, M.; Guagagnini, L.; Fiddy, S.G.; Santini, C.; Pellei, M. Cu K-edge EXAFS on copper(I) complexes containing dihydridobis(3-nitro-1,2,4-triazol-1-yl)borate and bis(1,2,4-triazol-1-yl)acetate ligand: Evidence for the Cu–O interaction. *Polyhedron* **2009**, *28*, 3600–3606. [CrossRef]
28. Kunzl, V. A linear dependence of energy levels on the valence of elements. *Collect. Trav. Chim. Tchecoslov.* **1932**, *4*, 213.
29. Abuin, M.; Serrano, A.; Chaboy, J.; García, M.A.; Carmona, N. XAS study of Mn, Fe and Cu as indicators of historical glass decay. *J. Anal. At. Spectrom.* **2013**, *28*, 1118–1124. [CrossRef]